The Journal of Physical Chemistry Letters

Letter

Cite This: J. Phys. Chem. Lett. 2018, 9, 6750−6754

pubs.acs.org/JPCL

Kinetics of Ion-Exchange Reactions in Hybrid Organic−Inorganic Perovskite Thin Films Studied by In Situ Real-Time X-ray Scattering

Alessandro Greco,[†] Alexander Hinderhofer,*[,†] M. Ibrahim Dar,*[,‡] Neha Arora,[‡] Jan Hagenlocher,[†] Andrey Chumakov,[¶] Michael Grätzel,[‡] and Frank Schreiber[†]

[†]Institute for Applied Physics, University of Tübingen, Auf der Morgenstelle 10, 72076 Tübingen, Germany

[‡]Laboratory of Photonics and Interfaces, Institute of Chemical Sciences and Engineering, École Polytechnique Fédérale de Lausanne, CH-1015 Lausanne, Switzerland

[¶]European Synchrotron Radiation Facility, 71, Avenue des Martyrs, CS 40220, 38043 Grenoble Cedex 9, France

Supporting Information

ABSTRACT: The exchange of ions in hybrid organic−inorganic perovskites with the general formula $APbX_3$ (A = MA, FA; X = I, Cl, Br) is studied in five different systems using in situ real-time grazing incident X-ray diffraction (GIXD). In systems where the organic cation is exchanged, we find a continuous shift of the lattice parameter. The relative shift compared to the pure materials is used to quantify the exchange. Whether or not a conversion is possible, as well as the amount of exchanged cations, depends on the halide used. In the case of the interconversion of $MAPbI_3$ and $MAPbCl_3$, we observe a decay of the diffraction peaks of the original perovskite and the emergence of new peaks corresponding to the structure with the alternative halide. Moreover, we determined the relevant time scales of the growth and decay of the perovskite structures.

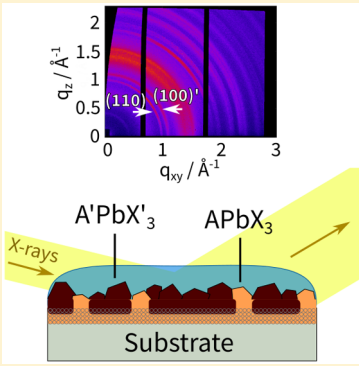

Hybrid organic−inorganic perovskite films with the general formula $APbX_3$ (A = CH_3NH_3, $CH(NH_2)_2$; X = I, Br, Cl) have received significant attention as absorber materials for photovoltaics.[1−6] Recent studies have shown that perovskite solar cells (PSCs) with high efficiencies can be created by mixing different halides[7,8] or by mixing different organic cations.[6,9,10] The use of multiple halides or cations can help tune the band gaps and improve the stability of perovskite films.[11−14] Furthermore, adding chloride or bromide to methylammonium lead iodide ($MAPbI_3$) has been shown to slow down the film growth and to improve the transport and diffusion lengths of charge carriers.[7,8,14−18]

A key point in this context is to understand the kinetic and energetic effects that determine how these ions mix and distribute in the film and how this affects the optoelectronic properties of the perovskite film. There are several preparation routes to create mixed perovskite films; one of these is the exchange of the ions in a pre-existing film by adding a solution containing different halides or organic cations.[19] In order to fully understand the exchange, real-time in situ characterization of the film is indispensable. Various halide exchanges as well as the $MAPbI_3$−$FAPbI_3$ interconversion (FA = $CH(NH_2)_2$) have already been studied with in situ photoluminescence and absorbance spectroscopy.[20] These methods, however, are unable to resolve the structural changes that occur in the perovskite film when ions are exchanged in the crystal lattice. In situ scattering experiments[21,22] are undoubtedly the method of choice to investigate these structural changes and their characteristic time scales.

In this work, we present a real-time study of five different perovskite conversions involving exchange of the organic cation or the halide. We employed in situ grazing incidence X-ray diffraction (GIXD) to investigate if an exchange is possible as well as the relevant time scales and the degree of exchange. The ion exchanges studied in this work are summarized in Table 1 and are divided into two types, namely, halide exchanges and cation exchanges.

The three different cation exchanges that have been studied in this work are the conversion of $MAPbBr_3$ to $FAPbBr_3$, the

Table 1. Summary of All Five Ion Exchanges with Their Initial Composition, Added Solution, and Final Composition[a]

initial	solution	final	exchange
$MAPbBr_3$	FABr	$MAPbBr_3$	no
$FAPbBr_3$	MABr	$MA_{0.35}FA_{0.65}PbBr_3$	yes
$MAPbI_3$	FAI	$MA_{0.4}FA_{0.6}PbI_3$	yes
$MAPbI_3$	MACl	$MAPbI_3/MAPbCl_3$	yes
$MAPbCl_3$	MAI	$MAPbI_3/MAPbCl_3$	yes

[a]The last column indicates if an exchange was at all possible.

Received: September 21, 2018
Accepted: October 23, 2018
Published: November 7, 2018

DOI: 10.1021/acs.jpclett.8b02916
J. Phys. Chem. Lett. 2018, 9, 6750−6754

inverse conversion of $FAPbBr_3$ to $MAPbBr_3$, and the conversion of $MAPbI_3$ to $FAPbI_3$. Figure 1 demonstrates the changing diffraction pattern in the reciprocal space maps (RSMs) before, during, and after conversion. The exchange of the ions was observed in real time by analyzing the integrated intensity and radial position of the Debye−Scherrer diffraction rings in the RSMs. The latter was done by fitting a Gaussian distribution to the azimuthally integrated radial profile of the Debye−Scherrer rings (demonstrated in detail in the Supporting Information).

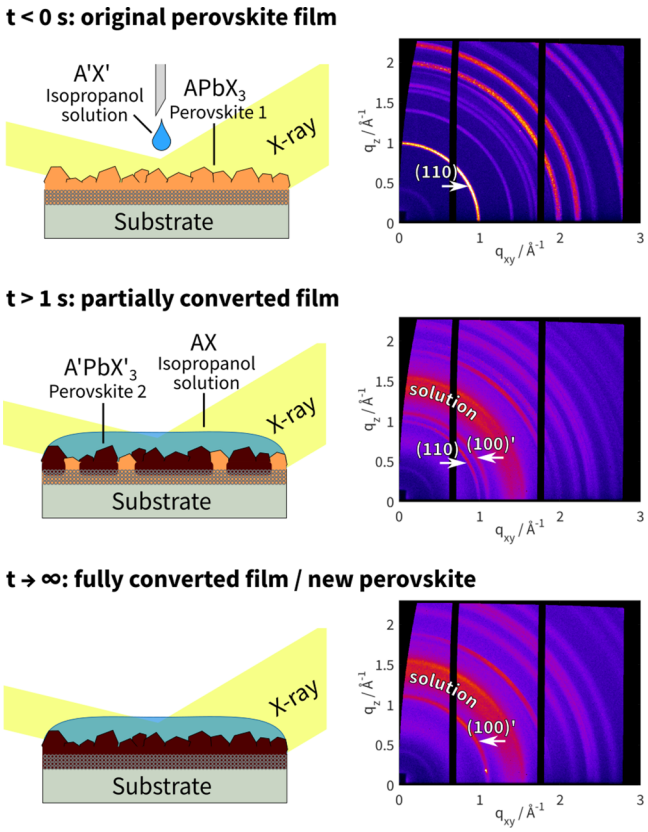

Figure 1. Right: RSMs before, during, and after the conversion of $MAPbI_3$ to $MAPbCl_3$. Left: Illustration to demonstrate the geometry of the experiment and the progress of the conversion. After addition of the solution, the characteristic (110) peak of $MAPbI_3$ starts to disappear and the corresponding $MAPbCl_3$ (100)′ peak starts to appear.

Figure 2a shows the average lattice parameters of the perovskite during the conversion of $MAPbBr_3$ to $FAPbBr_3$ and the conversion of $FAPbBr_3$ to $MAPbBr_3$. The lattice parameter during the conversion of $MAPbBr_3$ stays almost constant over the course of the experiment, whereas during the conversion of $FAPbBr_3$, it shows reduction toward that of pure $MAPbBr_3$. Although the observed shift is on the scale of roughly 1%, we trust its significance because it is continuous in time and on a length scale that is expected for FA−MA exchange. Assuming a linear relationship between the relative lattice parameter and the amount of exchanged cations (Vegard's law), the FA content of the perovskite during exchange can be calculated by comparing the lattice parameter of the mixed perovskite with those of the two pure perovskites, 5.96 and 6.04 Å, respectively. After 22 min, the perovskite has reached a nominal composition of $MA_{0.35}FA_{0.65}PbBr_3$, but the nonzero slope and exponentially decaying fit (red dashed line) of the lattice parameter in Figure 2a suggest that an even larger amount of the organic cations could be exchanged with longer reaction times. The characteristic decay time of τ = 709 s is comparable to what has been shown in previous ex situ studies of cation exchanges.[20] Because the exchange of MA by FA was not possible, we assume that in the $MA_xFA_{1-x}PbBr_3$ lattice pure $MAPbBr_3$ is likely to be energetically more stable than mixtures of FA and MA. However, it is important to stress that the exact composition of the film is also affected by kinetic effects such as, for example, the relative solubility of the original perovskite and the product and whether the exchange leads to a decrease or an increase of the molar volume.[23]

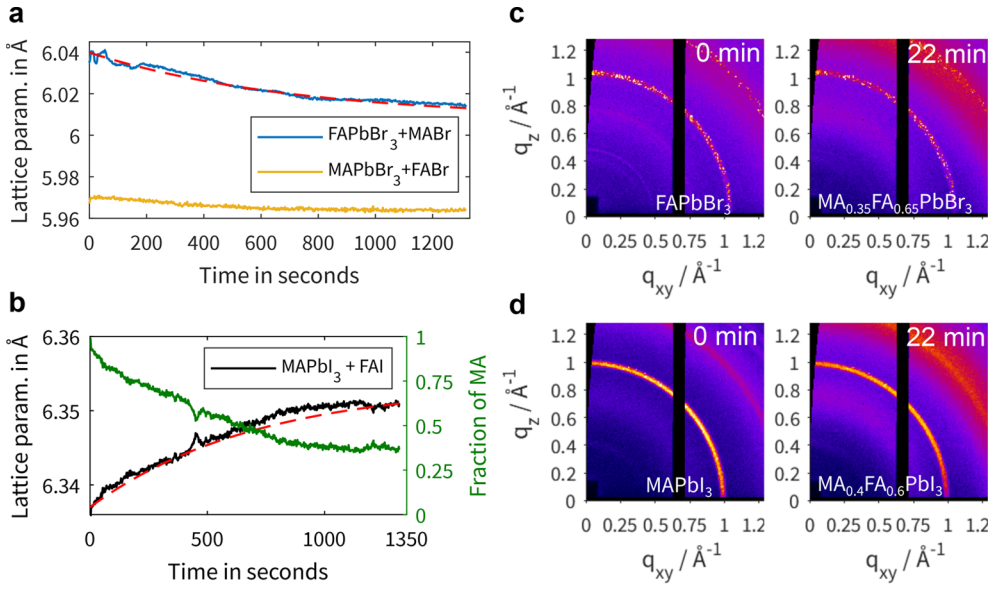

Figure 2. (a) Lattice parameter of the perovskite during the conversion of $FAPbBr_3$ to $MAPbBr_3$ and $MAPbBr_3$ to $FAPbBr_3$. Red dashed line: Decaying exponential fit ($a = a_0e^{t/\tau} + c$) with decay time τ = 709 s. (b) Black: Lattice parameter of the perovskite during the conversion of $MAPbI_3$ to $FAPbI_3$. Red dashed line: Decaying exponential fit ($a = a_0(1 - e^{t/\tau}) + c$) with decay time τ = 718 s. Green: MA content of the perovskite, i.e., x in $MA_xFA_{1-x}PbI_3$. (c,d) GIXD images of the (100)/(110) peak at the beginning and end of the conversion of $FAPbBr_3$ to $MAPbBr_3$ and $MAPbI_3$ to $FAPbI_3$, respectively.

DOI: 10.1021/acs.jpclett.8b02916
J. Phys. Chem. Lett. 2018, 9, 6750−6754

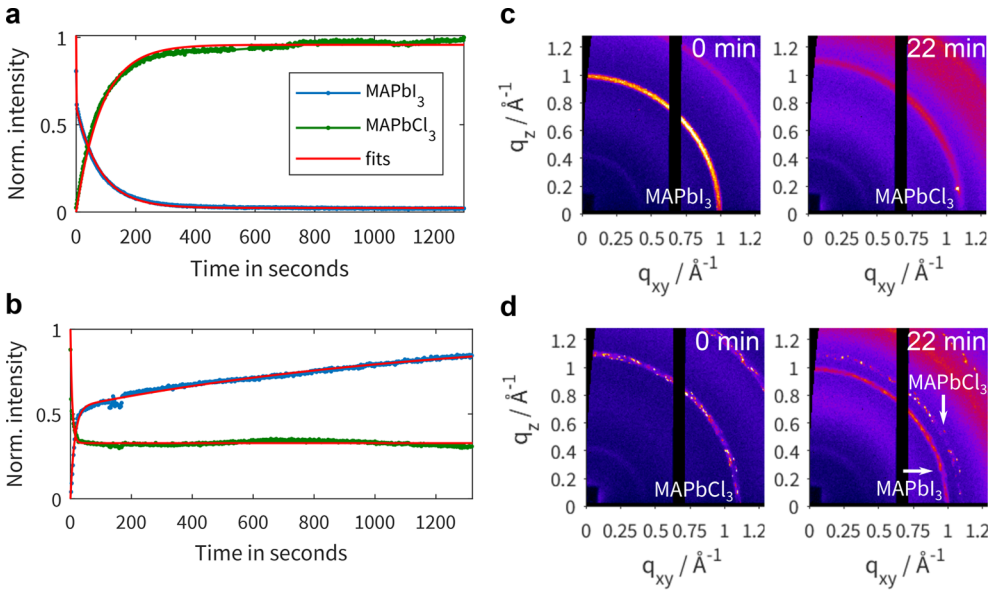

Figure 3. Integrated Bragg peak intensity of the $MAPbI_3$(110) and $MAPbCl_3$(100) structures during (a) the conversion of $MAPbI_3$ to $MAPbCl_3$ and (b) the conversion of $MAPbCl_3$ to $MAPbI_3$ (the legend applies to panels a and b). The curves were fitted with eqs 1 and 2, respectively. (c,d) GIXD images of the 110/100 peak at the beginning and end of the conversion of $MAPbI_3$ to $MAPbCl_3$ and $MAPbCl_3$ to $MAPbCl_3$, respectively.

In contrast to the $MAPbBr_3$−$FAPbBr_3$ system discussed above, the exchange of MA by FA was possible in $MAPbI_3$. Figure 2b shows the average lattice parameter (black curve) and the remaining MA content (green curve) of the perovskite against time. The lattice parameter moves from that of the pure material, 6.33 Å, to a higher value closer to that of $FAPbI_3$, 6.36 Å. Within 22 min, the exchange reaction saturates at a composition of $MA_{0.4}FA_{0.6}PbI_3$, i.e., over half of the MA is exchanged with FA. Furthermore, the exponentially decaying fit (red dashed line) yields a characteristic decay time of $\tau = 718$ s, which is very similar to the exchange of FA with MA in the bromide system. Considering that cubic $FAPbI_3$ is unstable at room temperature, this means that a mixture of FA and MA likely creates an energetically more stable perovskite lattice compared to those with either pure FA or MA.

In addition to the cation exchanges, two different halide exchanges have been studied, namely, the conversion of $MAPbI_3$ to $MAPbCl_3$ and the conversion of $MAPbCl_3$ to $MAPbI_3$. Both exchanges exhibit an intensity decrease of the Bragg reflections of the original perovskite and emergence of new peaks corresponding to the respective other perovskite. This means that two separate perovskite phases are present, which is in accordance with previous studies[19,24−26] and constitutes a notable qualitative difference to the previously shown cation exchanges where only continuous peak shifts are observed.

Figure 3a shows the integrated peak intensities of both phases against time during the conversion of $MAPbI_3$ to $MAPbCl_3$. The intensities have been normalized to their maximum value to highlight the progress of the exchange. Instead of a gradual peak shift, the formation of a new $MAPbCl_3$ phase is observed. By the end of the experiment, both the growth of the new phase and the decline of the original $MAPbI_3$ phase have saturated, which indicates complete conversion of the perovskite. To be able to quantify the growth and decay kinetics of the two structures, the $I(t)$ curves of the Bragg peak intensity were fitted with the growth laws

$$I(t) = A(1 - e^{-t/\tau}) \quad (1)$$

and

$$I(t) = Ae^{-t/\tau} + c \quad (2)$$

respectively. The fits yielded characteristic time constants τ (Table 2), which help to compare the kinetics of the crystal growth and decay. We note, however, that the $I(t)$ curves of the growing and declining phase show a pronounced asymmetry, which means that upon applying the solution part of the perovskite transitions into an intermediate phase that does not contribute to the intensity of any perovskite peak. The presence of an amorphous phase during the $MAPbI_3$−$MAPbCl_3$ interconversion has been described previously.[19] In the case of the conversion of $MAPbI_3$ to $MAPbCl_3$, we observe very similar time constants for both the decay of $MAPbI_3$ and the growth of $MAPbCl_3$, but we also observe a drop of the $MAPbI_3$ intensity immediately (∼2 s) after applying the solvent. This drop cannot be described by eq 2, and we attribute it to the transition into an amorphous phase.

Table 2. Time Constants Obtained from Fits of the Integrated Peak Intensity against Time (Equations 1 and 2)[a]

	$MAPbI_3$ + MACl		$MAPbCl_3$ + MAI	
	$MAPbI_3$ (decaying)	$MAPbCl_3$ (growing)	$MAPbCl_3$ (decaying)	$MAPbI_3$ (growing)
τ	82.5 ± 0.5	85.8 ± 1.2	5.99 ± 0.32	14.02 ± 0.52

[a]The error is expressed as the 95% confidence interval given by the fit (the systematic and statistical errors are likely somewhat higher).

During the inverse conversion of $MAPbCl_3$ to $MAPbI_3$, we also observe a decay of the Bragg peak intensity of the original perovskite and the emergence of new $MAPbI_3$ peaks (Figure 3b). The time constants of the growth law fits of the $I(t)$ curves are shown in Table 2. Overall, the growth and decay times for the two structures are lower (faster) than those during the inverse conversion of $MAPbI_3$ to $MAPbCl_3$. Furthermore, the rapid decay of $MAPbCl_3$ saturates within about 20 s at about 37% of its original intensity, which indicates that complete conversion was

DOI: 10.1021/acs.jpclett.8b02916
J. Phys. Chem. Lett. 2018, 9, 6750−6754

not possible. The remaining volume of $MAPbCl_3$ is perhaps kinetically trapped by the outer perovskite layers that prevent the necessary expansion of the molar volume and hinder the transport of ions through the film. Compared with the fast decay of $MAPbCl_3$, the initial growth of $MAPbI_3$ yields a similar time constant but is then followed by a period of slower growth. This slower growth is still ongoing by the end of the experiment and may be due to a transition of the intermediate amorphous phase into the crystalline phase of $MAPbI_3$. A second decaying exponential term with a time constant of τ_{slow} = 1250 s was needed to properly describe this transition.

In this study, we successfully tracked the in situ perovskite conversion of three cation exchanges and two halide exchanges. In bromide-based perovskite films, the exchange of FA with MA was possible, while the inverse exchange was not observed. This indicates that in this system pure $MAPbBr_3$ is energetically most stable. In the iodide-based perovskite, an exchange of MA with FA was possible, which saturated at a ratio of roughly 1:1. While the exact composition of the films is certainly affected by kinetic effects, such as limiting transport mechanisms, we conclude that, in contrast to the bromide-based perovskite, mixtures of MA and FA are more stable than pure $MAPbI_3$.

In contrast, the interconversion of $MAPbI_3$ and $MAPbCl_3$ showed a decrease of the Bragg peak intensity of the original perovskite as well as emergence of a new perovskite phase containing the added halide. During the conversion of $MAPbI_3$ to $MAPbCl_3$, the growth and decay of both structures happened on a similar time scale ($\tau \approx 80$ s), and a complete conversion was possible. The inverse conversion was significantly faster ($\tau \approx 10$ s), which highlights the importance of the amorphous intermediate phase on the exchange kinetics. In both cases, the respective growth and decay kinetics showed a pronounced asymmetry, which we attribute to the fast partial transition into an intermediate amorphous phase in the beginning, which then transitions into the crystalline perovskite phase on a slower time scale.

Although the exact time constants and amounts of exchanged ions will certainly depend on various experimental conditions, such as the concentration of the added solution and the coating method, the results presented in this work should give important insights into the structure formation and ion exchange kinetics of perovskite conversions.

EXPERIMENTAL SECTION

Materials. The solvents and lead halide salts were purchased from Acros Organics and Tokyo Chemical Industry, respectively. The organic cation salts were purchased from Dyesol. All were used as received.

Ion Exchange. A 200 μL 50 mM 2-propanol solution of A′X (cation exchange) or AX′ (halide exchange) was drop-cast onto a previously deposited $APbX_3$ film (t = 0 in all plots).

Structural Characterization. The GIXD experiments were performed at the European Synchrotron Radiation Facility at the ID10B beamline with a photon energy of 22 keV. The angle of incidence was 0.14°. The detector was a Pilatus300K (resolution: 487 × 619 pixels; pixel size: 0.172 mm) with a sample−detector distance of 472 mm. The integration time for each image was 2 s. The sample was kept under a nitrogen atmosphere during the measurement.

ASSOCIATED CONTENT

Supporting Information

The Supporting Information is available free of charge on the ACS Publications website at DOI: 10.1021/acs.jpclett.8b02916.

Available real-time reciprocal space map animations (ZIP)

Azimuthally integrated $I(q)$ profiles of all conversions, experimental details, including photoanode and perovskite film deposition, and estimation of the X-ray absorption of the solution (PDF)

AUTHOR INFORMATION

Corresponding Authors

*E-mail: alexander.hinderhofer@uni-tuebingen.de (A.H.).
*E-mail: ibrahim.dar@epfl.ch (M.I.D.).

ORCID

Alessandro Greco: 0000-0002-3714-7941
Alexander Hinderhofer: 0000-0001-8152-6386
M. Ibrahim Dar: 0000-0001-9489-8365
Michael Grätzel: 0000-0002-0068-0195

Notes

The authors declare no competing financial interest.

ACKNOWLEDGMENTS

The authors acknowledge support from the Deutsche Forschungsgemeinschaft. M.I.D and M.G. acknowledge financial support from KACST. M.I.D. acknowledges financial support from the Swiss National Science Foundation under the grant number P300P2_174471. N.A. acknowledges financial support from the Greatcell Solar. We also thank Michael Zimmermann for his contribution to the data analysis.

REFERENCES

(1) Arora, N.; Dar, M. I.; Hinderhofer, A.; Pellet, N.; Schreiber, F.; Zakeeruddin, S. M.; Grätzel, M. Perovskite solar cells with CuSCN hole extraction layers yield stabilized efficiencies greater than 20%. *Science* **2017**, *358*, 768−771.

(2) Snaith, H. J. Perovskites: the emergence of a new era for low-cost, high-efficiency solar cells. *J. Phys. Chem. Lett.* **2013**, *4*, 3623−3630.

(3) Green, M. A.; Ho-Baillie, A.; Snaith, H. J. The emergence of perovskite solar cells. *Nat. Photonics* **2014**, *8*, 506−514.

(4) Hodes, G.; Cahen, D. Photovoltaics: perovskite cells roll forward. *Nat. Photonics* **2014**, *8*, 87.

(5) Kim, H.-S.; Im, S. H.; Park, N.-G. Organolead halide perovskite: new horizons in solar cell research. *J. Phys. Chem. C* **2014**, *118*, 5615−5625.

(6) Bi, D.; Tress, W.; Dar, M. I.; Gao, P.; Luo, J.; Renevier, C.; Schenk, K.; Abate, A.; Giordano, F.; Baena, J.-P. C.; et al. Efficient luminescent solar cells based on tailored mixed-cation perovskites. *Science Advances* **2016**, *2*, e1501170.

(7) Ralaiarisoa, M.; Busby, Y.; Frisch, J.; Salzmann, I.; Pireaux, J.-J.; Koch, N. Correlation of annealing time with crystal structure, composition, and electronic properties of $CH_3NH_3PbI_{3-x}Cl_x$ mixed-halide perovskite films. *Phys. Chem. Chem. Phys.* **2017**, *19*, 828−836.

(8) Colella, S.; Mosconi, E.; Fedeli, P.; Listorti, A.; Gazza, F.; Orlandi, F.; Ferro, P.; Besagni, T.; Rizzo, A.; Calestani, G.; et al. $MAPbI_{3-x}Cl_x$ Mixed Halide Perovskite for Hybrid Solar Cells: The Role of Chloride as Dopant on the Transport and Structural Properties. *Chem. Mater.* **2013**, *25*, 4613−4618.

(9) Pellet, N.; Gao, P.; Gregori, G.; Yang, T.-Y.; Nazeeruddin, M. K.; Maier, J.; Grätzel, M. Mixed-organic-cation Perovskite photovoltaics for enhanced solar-light harvesting. *Angew. Chem., Int. Ed.* **2014**, *53*, 3151−3157.

DOI: 10.1021/acs.jpclett.8b02916
J. Phys. Chem. Lett. 2018, 9, 6750−6754

(10) Jeon, N. J.; Noh, J. H.; Yang, W. S.; Kim, Y. C.; Ryu, S.; Seo, J.; Seok, S. I. Compositional engineering of perovskite materials for high-performance solar cells. *Nature* **2015**, *517*, 476.
(11) Amat, A.; Mosconi, E.; Ronca, E.; Quarti, C.; Umari, P.; Nazeeruddin, M. K.; Grätzel, M.; De Angelis, F. Cation-induced band-gap tuning in organohalide perovskites: interplay of spin−orbit coupling and octahedra tilting. *Nano Lett.* **2014**, *14*, 3608−3616.
(12) Eperon, G. E.; Stranks, S. D.; Menelaou, C.; Johnston, M. B.; Herz, L. M.; Snaith, H. J. Formamidinium lead trihalide: a broadly tunable perovskite for efficient planar heterojunction solar cells. *Energy Environ. Sci.* **2014**, *7*, 982−988.
(13) Zheng, X.; Wu, C.; Jha, S. K.; Li, Z.; Zhu, K.; Priya, S. Improved phase stability of formamidinium lead triiodide perovskite by strain relaxation. *ACS Energy Letters* **2016**, *1*, 1014−1020.
(14) Ibrahim Dar, M.; Abdi-Jalebi, M.; Arora, N.; Moehl, T.; Grätzel, M.; Nazeeruddin, M. K. Understanding the impact of bromide on the photovoltaic performance of $CH_3NH_3PbI_3$ solar cells. *Adv. Mater.* **2015**, *27*, 7221−7228.
(15) Stranks, S. D.; Eperon, G. E.; Grancini, G.; Menelaou, C.; Alcocer, M. J.; Leijtens, T.; Herz, L. M.; Petrozza, A.; Snaith, H. J. Electron-hole diffusion lengths exceeding 1 micrometer in an organometal trihalide perovskite absorber. *Science* **2013**, *342*, 341−344.
(16) Williams, S. T.; Zuo, F.; Chueh, C.-C.; Liao, C.-Y.; Liang, P.-W.; Jen, A. K.-Y. Role of chloride in the morphological evolution of organo-lead halide perovskite thin films. *ACS Nano* **2014**, *8*, 10640−10654.
(17) Docampo, P.; Hanusch, F. C.; Stranks, S. D.; Döblinger, M.; Feckl, J. M.; Ehrensperger, M.; Minar, N. K.; Johnston, M. B.; Snaith, H. J.; Bein, T. Solution deposition-conversion for planar heterojunction mixed halide perovskite solar cells. *Adv. Energy Mater.* **2014**, *4*, 1400355.
(18) Dar, M. I.; Abdi-Jalebi, M.; Arora, N.; Grätzel, M.; Nazeeruddin, M. K. Growth Engineering of $CH_3NH_3PbI_3$ Structures for High-Efficiency Solar Cells. *Adv. Energy Mater.* **2016**, *6*, 1501358.
(19) Pellet, N.; Teuscher, J.; Maier, J.; Grätzel, M. Transforming hybrid organic inorganic perovskites by rapid halide exchange. *Chem. Mater.* **2015**, *27*, 2181−2188.
(20) Eperon, G. E.; Beck, C. E.; Snaith, H. J. Cation exchange for thin film lead iodide perovskite interconversion. *Mater. Horiz.* **2016**, *3*, 63−71.
(21) Kowarik, S. Thin film growth studies using time-resolved x-ray scattering. *J. Phys.: Condens. Matter* **2017**, *29*, 043003.
(22) Pistor, P.; Burwig, T.; Brzuska, C.; Weber, B.; Fränzel, W. Thermal stability and miscibility of co-evaporated methyl ammonium lead halide ($MAPbX_3$, X= I, Br, Cl) thin films analysed by in situ X-ray diffraction. *J. Mater. Chem. A* **2018**, *6*, 11496−11506.
(23) Putnis, A.; Putnis, C. V. The mechanism of reequilibration of solids in the presence of a fluid phase. *J. Solid State Chem.* **2007**, *180*, 1783−1786.
(24) Dualeh, A.; Tétreault, N.; Moehl, T.; Gao, P.; Nazeeruddin, M. K.; Grätzel, M. Effect of annealing temperature on film morphology of organic−inorganic hybrid pervoskite solid-state solar cells. *Adv. Funct. Mater.* **2014**, *24*, 3250−3258.
(25) Yu, H.; Wang, F.; Xie, F.; Li, W.; Chen, J.; Zhao, N. The Role of Chlorine in the Formation Process of "$CH_3NH_3PbI_{3-x}Cl_x$" Perovskite. *Adv. Funct. Mater.* **2014**, *24*, 7102−7108.
(26) Dar, M. I.; Arora, N.; Gao, P.; Ahmad, S.; Grätzel, M.; Nazeeruddin, M. K. Investigation regarding the role of chloride in organic−inorganic halide perovskites obtained from chloride containing precursors. *Nano Lett.* **2014**, *14*, 6991−6996.

DOI: 10.1021/acs.jpclett.8b02916
J. Phys. Chem. Lett. 2018, 9, 6750−6754